https://doi.org/10.31436/iiumej.v27i2.4008

Raindrop Size Distribution and Wind-Driven Rain Specific Attenuation: CCDF-Based Analysis at 18 and 38 GHz in Tropical Country

NURUL NAJWA MD YUSOF[1,3], OMAR ABDUL AZIZ[1]*, LAM HONG YIN[2], JAFRI DIN[1]

[1]*Faculty of Engineering, Universiti Teknologi Malaysia, Johor Bahru, Malaysia*
[2]*Faculty of Engineering Technology, Universiti Tun Hussein Onn Malaysia, Batu Pahat, Malaysia*
[3]*Polytechnic and Community College Education Department, Ministry of Higher Education, Putrajaya, Malaysia*

**Corresponding author: omar@utm.my*

(Received: 23 October 2025; Accepted: 8 March 2026; Published online: 10 May 2026)

ABSTRACT: Seasonal monsoons, frequency dependence, and wind effects were investigated for rain-specific attenuation at millimeter-wave (mm-wave) frequencies in a tropical environment. Using one-minute RD-69 DSD data and matched wind observations, CCDFs of specific attenuation were evaluated at 18 and 38 GHz for three monsoon phases (SW, NE, IM) and four wind-direction sectors under unconstrained and constrained winds (9–11 m/s). The CCDF results show clear seasonal variability, with the SW monsoon producing the strongest attenuation and the largest mismatch from ITU-R P.838-3, particularly at 38 GHz. Error statistics show that the maximum deviation occurs in the SW 270°–360° sector, with an RMSE of 1.550 dB/km and a positive bias, confirming ITU-R underestimation. Meanwhile, the NE monsoon exhibits smaller overall deviations (worst-case RMSE below about 0.6 dB/km at 38 GHz). The IM period exhibits mixed behavior, where wind direction can shift the deviation between under- and overestimation under constrained winds. Exceedance levels of 0.01% and 0.001% were emphasized as design-relevant extremes, corresponding to approximately 52.6 min/year and 5.26 min/year, respectively, under one-minute sampling. Overall, the results indicate that ITU-R P.838-3 accuracy in tropical conditions depends on monsoon phase and wind direction, supporting monsoon-aware, direction-sensitive fade-margin planning and link-orientation considerations for robust 5G/6G terrestrial mm-wave systems.

ABSTRAK: Monsun bermusim, kebergantungan frekuensi, dan kesan angin telah dikaji terhadap pelemahan spesifik hujan pada frekuensi gelombang milimeter (mm-wave) dalam persekitaran tropika. Menggunakan data DSD RD-69 beresolusi satu minit dan melalui pemerhatian padanan angin, pelemahan CCDF spesifik dinilai pada 18 dan 38 GHz untuk tiga fasa monsun (SW, NE, IM) dan empat sektor arah angin di bawah angin tidak terkekang serta angin terkekang (9–11 m/s). Penyimpangan terbesar daripada ITU-R P.838-3 berlaku pada 38 GHz, khususnya semasa monsun barat daya (SW), apabila sektor 270°–360° di bawah angin tidak terkekang menunjukkan RMSE = 1.550 dB/km dan bias = +1.193 dB/km, menandakan ITU-R bernilai lebih rendah; di bawah angin terkekang, penyimpangan kekal tinggi (RMSE = 1.383 dB/km). Tempoh peralihan (IM) juga menunjukkan kebergantungan pada sektor angin terkekang, dengan RMSE = 1.212 dB/km dan bias = +0.936 dB/km pada 38 GHz, manakala monsun timur laut (NE) menunjukkan penyimpangan lebih kecil (RMSE terburuk adalah kurang daripada kira-kira 0.6 dB/km pada 38 GHz di bawah angin tidak terkekang). Tahap kebarangkalian lebihan 0.01% dan 0.001% ditekankan sebagai ekstrem yang relevan bagi reka bentuk, bersamaan kira-kira 52.6 min/tahun dan 5.26 min/tahun, masing-masing, pada pensampelan satu minit. Secara keseluruhan, dapatan kajian menunjukkan ketepatan ITU-R P.838-3 dalam keadaan tropika bergantung pada fasa monsun dan arah angin,

sekaligus menyokong perancangan margin-pudaran yang peka monsun dan peka arah angin serta menimbang orientasi pautan untuk sistem gelombang-mm 5G/6G terestrial yang lebih berdaya tahan.

KEYWORDS: *raindrop size distribution, DSD, specific attenuation, millimeter-wave*

1. INTRODUCTION

Millimeter-wave (mm-wave) link development is gaining attention for its application in fifth- and sixth-generation (5G/6G) high-capacity cellular services. Nevertheless, communication in this frequency range is susceptible to rain attenuation, particularly in tropical environments with convective thunderstorms that produce very large raindrops. Absorption and scattering of wireless signals are affected by raindrop size as well as the signal's wavelength. Given that specific attenuation increases with frequency, the 18–40 GHz spectrum is particularly vulnerable to the effects of tropical rain microphysics [1]. Communication links operating at 38 GHz and beyond are further degraded by depolarization caused by oblate convective raindrop shapes during thunderstorms [2]. The aforementioned scenarios are typical of Malaysia's tropical climates. Considering the standard 1-minute time interval, Malaysia experiences rain rates exceeding 100 mm/h for 0.01% of the time, which is among the highest in the world [3-4]. Local Malaysian measurements recorded a greater concentration and wider range in the raindrop size distribution (DSD) than in temperate climates. This contributes to the rainy season's decaying profile with higher specific attenuation at 18/38 GHz [5-6], As reported in [7-8], rain-induced attenuation measurements at 18 GHz and 38 GHz recorded 33 dB and 21 dB, respectively, during the 0.01% worst-case operational time in Malaysia. Since most standard prediction tools for mm-wave links, including models from the International Telecommunication Union Radiocommunication (ITU-R), are primarily based on temperate-region data, calibration and correction of these models with respect to tropical data are necessary [9-10].

The 38 GHz band has been allocated for mm-wave 5G [7], while the 18 GHz band is under serious consideration for the upcoming 6G [11]. Verifying the channels' potential coverage distance is therefore critical when planning future cellular networks [12-13]. Given the importance of both bands for terrestrial point-to-point and fixed network access systems, their operation has been considered in the ITU-R P.530 standard model when rainfall occurs [14, 14]. However, for prediction models to closely resemble actual cases, rain rate and DSD data for the specific region should be used based on tropical climate samples [16-17]. Most previous works have concentrated on frequency scaling and variability driven by DSD and have largely treated precipitation as isotropic and time-invariant, which is not the case. Wind, in both speed and direction, as well as the monsoon phase, dramatically influences the shape, orientation, and alignment of raindrops. This creates direction-dependent attenuation that most models do not account for [18-20]. These gaps can cause systematic fade-margin shortfalls during extreme rain events, putting link reliability at risk of not meeting the availability targets expected of 5G and 6G backhaul.

The need to investigate the combined influence of the monsoon season, wind direction, and wind speed on specific attenuation at 18 GHz and 38 GHz is therefore essential. This paper closes this gap by investigating rain attenuation, accounting for seasonal monsoon, wind vectors, and DSD microphysics to quantify exceedance-level behavior. This study aims to provide a comprehensive assessment of standard rain-specific attenuation in tropical conditions, namely the ITU-R model, to formulate a monsoon-aware, direction-dependent fade-margin framework that improves 5G link design and future sub-terahertz 6G system

planning [6,7,21]. The remainder of this paper is organized as follows. Section 2 presents the methodology, including the RD-69 DSD dataset, the data extraction strategy, wind-constraint classification, the specific attenuation computation using both ITU-R P.838-3 and the DSD-derived specific attenuation, and the CCDF construction procedure. Section 3 reports and discusses the CCDF results across monsoon phases and wind-direction sectors, supported by RMSE and bias statistics for model comparison. Section 4 concludes the paper by summarizing the key findings and their implications for mm-wave fade-margin planning and link-orientation considerations for 5G/6G deployments in tropical climates.

2. METHODOLOGY

Three years of DSD data in this study were measured using the RD-69 Joss-Waldvogel disdrometer model. This disdrometer is located at Universiti Teknologi Malaysia, Kuala Lumpur, and is capable of measuring rainfall attributes, drop size, and the interval to enable high-resolution measurements. It identifies and classifies individual drops by size, from 0.36 to 5.30 mm, and by fall velocity as they traverse a sensing zone, sorting them into 20 different bins. The RD-69 disdrometer captures finer details of the DSD over time and ensures reliable, precise measurements. For the RD-69 disdrometer, a conical styrofoam collector is positioned over the sensing unit. This collector reduces wind effects and ensures that raindrops fall vertically onto the sensor. The sensing unit is a coil of wire suspended within a magnetic field.

A moving coil is the result of a droplet striking the collector. This movement activates the sensor, and a designed measuring device is created, where the data logger captures the corresponding voltage. The disdrometer captures the DSD from the voltage pulses produced by the RD-69 disdrometer. The size of each pulse indicates the size of the corresponding raindrop. The number of pulses corresponding to each size category is divided by the sampling interval to obtain the rainfall rate in mm/h. More information on the measurement setup is described in [22]. To ensure consistency across seasons, the dataset was grouped into three monsoon phases: Southwest (SW) monsoon, Northeast (NE) monsoon, and Intermonsoon (IM). Wind direction was further grouped into four sectors (0°–90°, 90°–180°, 180°–270°, and 270°–360°) to enable a directional comparison of rain microphysics and the corresponding specific attenuation.

2.1. Data Extraction Strategy

For each monsoon phase and wind direction, contiguous 20-minute windows were extracted from the one-minute DSD and wind records. This window length is suitable for tropical rainfall because it is short enough to capture rapid temporal changes in rainfall intensity and the associated evolution of the DSD during different phases of a rain event, yet long enough to provide a sufficient sample size for stable exceedance statistics after stratification [23]. To ensure comparability across categories and to focus on operationally relevant intense rain, only windows with a mean rainfall rate of 40–50 mm/h were retained, where the mean was computed as the arithmetic average of the 20 one-minute rainfall rates. Limiting the analysis to a narrow rain-rate range also makes the comparison fairer because the results are less influenced by changes in rainfall intensity and more related to DSD variability and wind conditions [24]. Windows with missing DSD or wind records were discarded. Wind speed and wind direction were obtained from the Malaysian Meteorological Department (MET Malaysia) and matched to the same observation periods as the DSD records. Tables 1–3 summarize the average drop counts for the SW, NE, and IM periods, respectively, stratified by wind-direction sector under both unconstrained winds and constrained winds (9–11 m/s).

https://doi.org/10.31436/iiumej.v27i2.4008

Table 1. Average drop counts during the SW monsoon under unconstrained winds and constrained winds (9–11 m/s).

Bin Number	Mean Diameter [mm]	Unconstrained winds				Constrained winds (9-11 m/s)			
		SW				SW			
		0° - 90°	90° - 180°	180° - 270°	270° - 360°	0° - 90°	90° - 180°	180° - 270°	270° - 360°
1	0.36	7	4	6	4	7	1	7	0
2	0.46	10	17	13	14	10	1	12	1
3	0.55	17	28	17	35	17	4	19	8
4	0.66	41	44	26	64	41	5	35	23
5	0.77	50	45	31	75	50	7	43	33
6	0.91	118	105	90	139	118	43	118	95
7	1.12	183	175	168	189	183	117	188	141
8	1.33	142	137	123	142	142	99	144	108
9	1.51	105	97	90	107	105	71	100	78
10	1.67	97	88	79	108	97	60	80	65
11	1.91	135	142	105	159	135	83	115	91
12	2.26	93	91	70	121	93	62	80	74
13	2.58	43	42	38	59	43	38	41	39
14	2.87	27	27	26	33	27	23	29	24
15	3.20	21	22	21	24	21	23	27	22
16	3.54	13	11	12	11	13	14	15	15
17	3.92	6	8	12	5	6	13	11	9
18	4.35	2	3	7	2	2	9	5	4
19	4.86	1	2	4	1	1	6	2	3
20	5.30	0	1	2	0	0	3	1	1

2.2. Wind Constraint Classification

To assess the effect of wind, the DSD samples were separated into two groups, considering wind speed: (i) unconstrained wind, which includes all retained segments regardless of wind speed, and (ii) constrained wind, which includes only segments with wind speeds of 9–11 m/s. Wind speeds in Malaysia are influenced by monsoon seasons, with significant variability throughout the year. The NE monsoon, in particular, brings higher wind speeds. Selecting a range of 9–11 m/s would capture the upper end of typical wind speeds during these periods, providing a realistic scenario for studying wind effects on mm-wave propagation. Furthermore, wind speeds in this range can cause antenna misalignment due to wind-induced vibrations, which is critical for maintaining the reliability of mm-wave communication links [25]. Therefore, analyzing this regime provides practical guidance for mitigation and more robust link planning.

2.3. Specific Attenuation Computation

This study assesses two methods to calculate specific attenuation. Specific attenuation, γ (dB/km), was computed using two approaches: (i) the standard ITU-R P.838-3 power-law model, and (ii) a DSD-derived specific attenuation based on the forward scattering amplitude (FSA) obtained via the T-matrix method. The ITU-R standard has established a widely recognized method for calculating specific attenuation as a function of frequency and rain rate. This method offers a reliable means of estimating the attenuation of the rain-induced signal. The ITU-R P.838-3 equation can be written as described in Eq. (1), where R is the rainfall rate (mm/h), and k and α are frequency and polarization-dependent.

$$\gamma = kR^{\alpha} \text{ (dB/km)} \quad (1)$$

https://doi.org/10.31436/iiumej.v27i2.4008

Specific attenuation was also computed directly from the measured DSD using a T-matrix approach. In this method, the complex forward-scattering amplitude (FSA) is computed for each drop-diameter bin and summed over all bins to obtain the specific attenuation per unit length, as given in Eq. (2). This DSD-derived specific attenuation captures microphysical variability that is not represented by rainfall-rate-only models and enables a physically consistent comparison with the ITU-R prediction.

$$\gamma_{H,V} = 8.686 \times 10^3 \times \lambda \times \sum_{i=1}^{20} Im\{f_{H,V}(D_i)\} \cdot N(D_i) \cdot \Delta D_i \text{ (dB/km)} \quad (2)$$

where λ is the wavelength (m), $Im\{\cdot\}$ denotes the imaginary part, $f_{H,V}(D_i)$ is the T-matrix derived forward-scattering amplitude for drop diameter D_i, $N(D_i)$ is the drop concentration for bin i ($m^{-3}mm^{-1}$), and ΔD_i is the bin width in mm. The constant in (2) provides conversion to dB/km under the units defined above. The T-matrix method is used to compute $Im(f_{H,V}(D_i))$ for each diameter bin, allowing the attenuation to be driven directly by the observed DSD rather than by rainfall rate alone [6].

The bin-wise drop-count distributions used to support the DSD-derived attenuation calculation are summarized in Tables 2 and 3. Table 2 presents the average drop counts during the northeast (NE) monsoon, while Table 3 presents the corresponding values during the inter-monsoon (IM) period. In both tables, the drop counts are grouped according to mean drop diameter, wind-direction sector, and wind-speed condition, namely unconstrained winds and constrained winds within 9–11 m/s. These distributions provide the microphysical basis for estimating $N(D_i)$ in Eq. (2), enabling the attenuation calculation to reflect seasonal and wind-dependent variations in the observed DSD.

Table 2. Average drop counts during the NE monsoon under unconstrained and constrained winds (9–11 m/s).

Bin Number	Mean Diameter [mm]	Unconstrained winds				Constrained winds (9-11 m/s)			
		NE				NE			
		0° - 90°	90° - 180°	180° - 270°	270° - 360°	0° - 90°	90° - 180°	180° - 270°	270° - 360°
1	0.36	9	3	10	1	10	6	0	6
2	0.46	40	10	31	6	25	17	2	14
3	0.55	71	19	38	23	28	27	14	20
4	0.66	98	40	56	51	33	51	36	30
5	0.77	93	44	53	60	29	56	61	29
6	0.91	181	114	132	135	97	131	134	74
7	1.12	270	199	210	188	220	214	201	152
8	1.33	186	140	163	136	166	172	133	133
9	1.51	119	102	99	102	116	124	94	97
10	1.67	105	97	91	93	100	110	91	82
11	1.91	141	139	121	135	123	147	141	122
12	2.26	97	92	79	103	77	96	99	79
13	2.58	45	44	37	46	38	45	56	41
14	2.87	26	27	24	26	24	29	34	28
15	3.20	22	19	22	20	21	21	26	24
16	3.54	11	10	11	9	15	8	11	12
17	3.92	7	6	9	7	11	6	6	9
18	4.35	3	2	4	3	4	2	2	4
19	4.86	1	1	2	1	2	1	0	2
20	5.30	0	0	1	0	0	0	0	1

https://doi.org/10.31436/iiumej.v27i2.4008

Table 3. Average drop counts during IM monsoon under unconstrained winds and constrained winds (9–11 m/s).

Bin Number	Mean Diameter [mm]	Unconstrained winds				Constrained winds (9-11 m/s)			
		IM				IM			
		0° - 90°	90° - 180°	180° - 270°	270° - 360°	0° - 90°	90° - 180°	180° - 270°	270° - 360°
1	0.36	6	20	1	0	4	3	5	1
2	0.46	24	38	8	4	12	11	14	4
3	0.55	36	39	48	19	21	26	21	18
4	0.66	62	58	90	47	40	45	32	43
5	0.77	59	62	94	52	50	47	38	51
6	0.91	126	154	184	118	120	106	95	117
7	1.12	192	247	230	182	189	184	164	186
8	1.33	141	177	170	134	153	141	136	131
9	1.51	97	113	109	99	116	97	96	100
10	1.67	87	94	97	93	112	86	86	95
11	1.91	128	131	131	141	180	120	130	144
12	2.26	89	92	88	93	115	78	95	95
13	2.58	45	43	48	40	56	42	43	42
14	2.87	32	25	29	27	32	30	23	28
15	3.20	27	23	23	19	18	26	20	21
16	3.54	13	12	9	8	6	12	11	10
17	3.92	7	7	5	6	3	8	8	7
18	4.35	2	3	1	3	1	3	4	4
19	4.86	0	1	0	2	0	1	2	2
20	5.30	0	0	0	1	0	0	1	1

2.4. CCDF Construction

In this study, the complementary cumulative distribution function (CCDF) was used to quantify the frequency with which the specific attenuation exceeds a given level under different monsoon and wind conditions. First, one-minute DSD measurements from the RD-69 disdrometer were used to derive a time series of specific attenuation, $\gamma(t)$, for each retained 20-minute window. The specific attenuation was computed using Eq. (1) and Eq. (2). The resulting $\gamma(t)$ samples were then grouped according to the analysis categories (monsoon phase, wind direction, and wind speed group). For each category, all specific attenuation samples were pooled and sorted, and the exceedance probability for any specific attenuation threshold x was evaluated as $P(\gamma \geq x)$, where $P(\cdot)$ denotes probability. In practice, it was estimated as the fraction of samples with γ greater than or equal to x. Plotting $P(\gamma \geq x)$ against x produced the CCDF curves, which were used to compare the DSD-derived specific attenuation statistics with the corresponding ITU-R predictions under the same conditions. Finally, exceedance levels at 0.01% and 0.001% were reported as reference points for link design. With one-minute sampling, these correspond to approximately 52.6 min/year and 5.26 min/year, respectively.

3. Results and Discussion

This study evaluates how monsoon phase and wind direction influence mm-wave specific attenuation in a tropical environment and whether ITU-R P.838-3 remains adequate when attenuation is derived from local DSD. The CCDF results show that agreement with ITU-R is not uniform across seasons or wind sectors, and the deviation is most pronounced at 38 GHz. This matters because 38 GHz is a key FR2 band where fade margins are typically tight; even sector-dependent differences of the order of 1 dB/km can accumulate into noticeable

https://doi.org/10.31436/iiumej.v27i2.4008

uncertainty for short-path terrestrial planning, especially at low time percentages relevant to high availability targets. To complement the CCDF comparisons, Tables 4 and 5 summarize the model deviations in terms of RMSE and bias between the DSD-derived attenuation and ITU-R P.838-3. A positive bias (+) indicates ITU-R underestimation, while a negative bias (−) indicates overestimation. In this context, bias explains the *direction* of the mismatch, whereas RMSE reflects the typical *magnitude* of the mismatch in dB/km across the evaluated sectors. This distinction is important because bias can appear small when under- and overestimation across directions partially cancel out, while RMSE still reveals substantial spread across sectors.

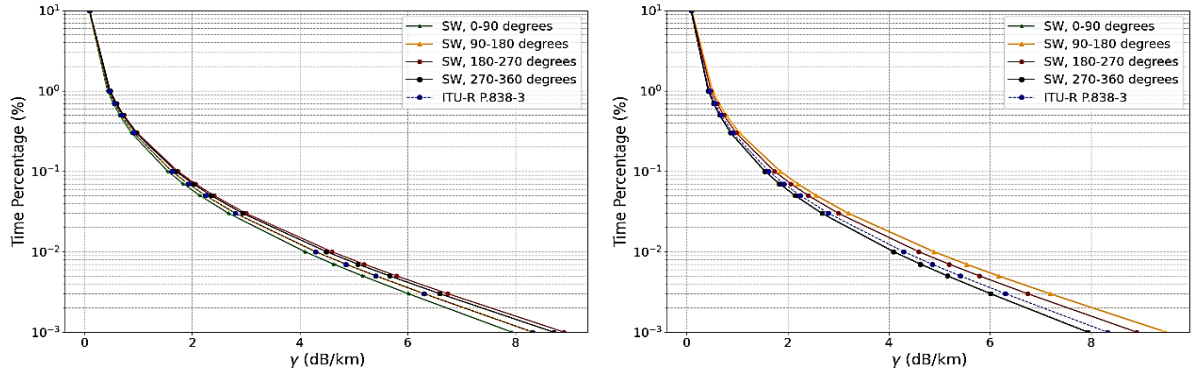

Figure 1. CCDF of specific attenuation (γ, dB/km) during the SW monsoon for 40–50 mm/h against ITU-R P.838-3 at 18 GHz under (a) unconstrained winds and (b) constrained winds (9–11 m/s)

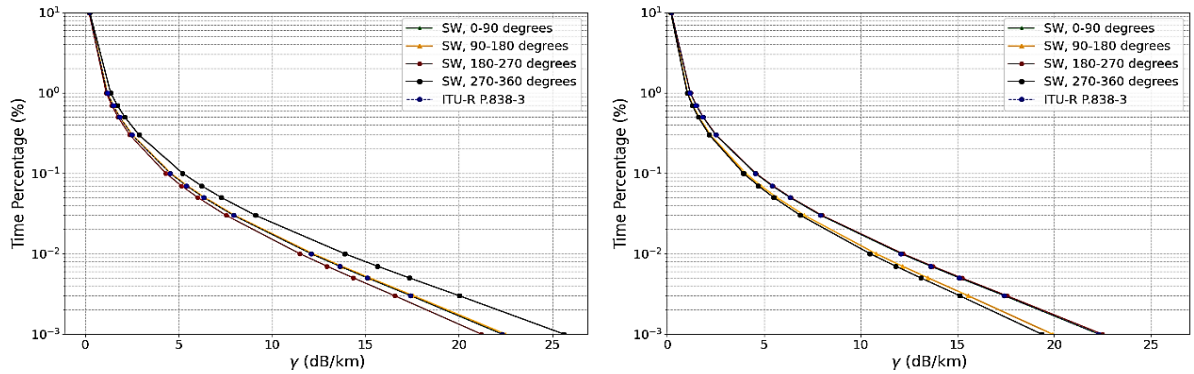

Figure 2. CCDF of specific attenuation (γ, dB/km) during the SW monsoon for 40–50 mm/h against ITU-R P.838-3 at 38 GHz under (a) unconstrained winds and (b) constrained winds (9–11 m/s)

During the SW monsoon, the CCDFs in Figure. 1 and 2 exhibit the widest directional spread and the clearest separation from the ITU-R curve, particularly at 38 GHz. This indicates that SW conditions produce stronger sensitivity to DSD variability and wind-driven microphysical effects, consistent with convective dominance in tropical rainfall [20]. Similar behavior has been reported for 32/38 GHz terrestrial links where rare-event attenuation exceeds theoretical predictions, suggesting the importance of local microphysics in model mismatch [12]. Local assessments in equatorial Malaysia also highlight persistent deviations even with recent ITU-R updates, reinforcing the need for local characterization in such climates [10]. The quantitative error statistics confirm this CCDF observation: at 38 GHz under unconstrained winds, the 270°–360° sector exhibits the largest mismatch, with RMSE = 1.550 dB/km and

bias = +1.193 dB/km (Table 4), indicating an ITU-R underestimation. Importantly, the bias is not uniform across directions; the 180°–270° sector shows the opposite tendency (bias = −0.393 dB/km, Table 4), meaning ITU-R can also overestimate depending on the wind sector. Under constrained winds (9–11 m/s), the deviation remains high in the 270°–360° sector (RMSE = 1.383 dB/km, Table 5). Overall, SW is the season with the most pronounced directional dependence, and reliance on a single rainfall-rate-based model can lead to the greatest planning uncertainty at 38 GHz.

In contrast, the NE monsoon CCDFs in Figures 3 and 4 remain close to ITU-R P.838-3 across most sectors under both wind classifications. This implies reduced direction-dependent variability compared with SW and suggests more stable attenuation behavior during NE. The error statistics support this: the 38 GHz RMSE remains comparatively modest, with the worst-case value staying below about 0.6 dB/km under unconstrained winds (Table 4), and bias values generally remain small in magnitude (Tables 4 and 5). In practice, this means ITU-R P.838-3 is more likely to provide an acceptable baseline for NE-season planning, with fewer sectors exhibiting large systematic offsets.

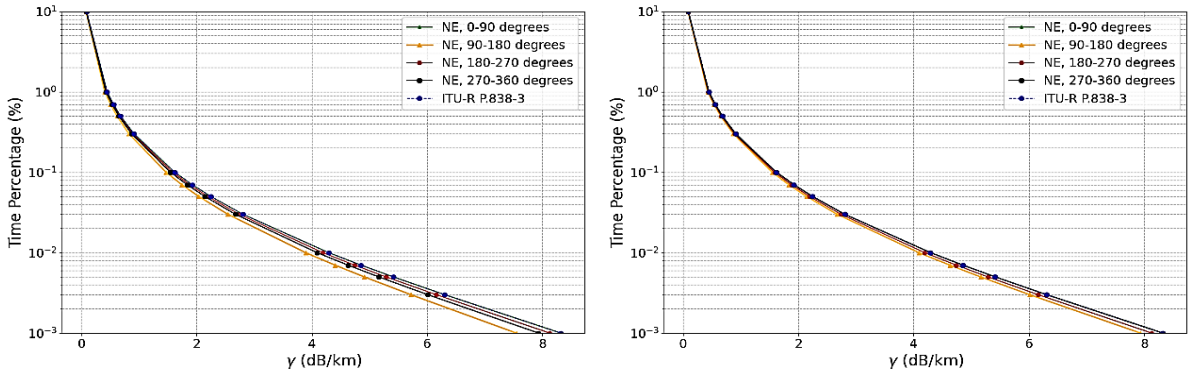

(a) (b)

Figure 3. CCDF of specific attenuation (γ, dB/km) during the NE monsoon for 40–50 mm/h against ITU-R P.838-3 at 18 GHz under (a) unconstrained winds and (b) constrained winds (9–11 m/s)

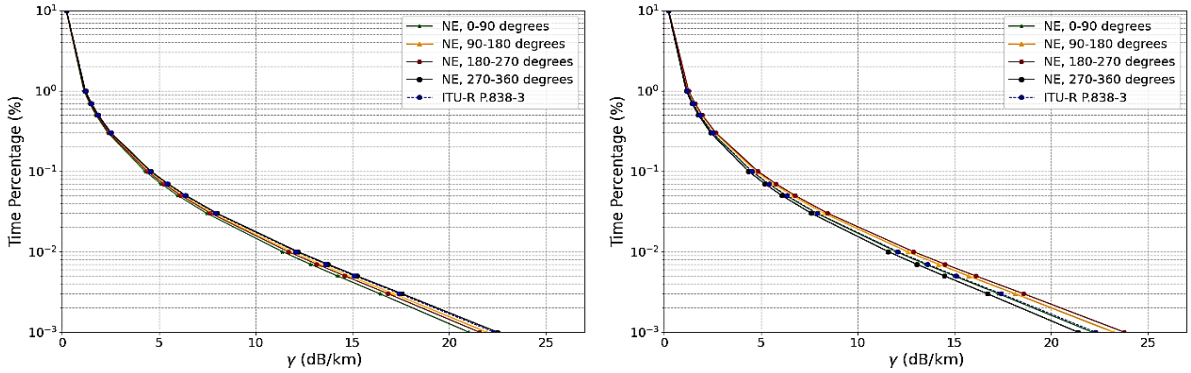

(a) (b)

Figure 4. CCDF of specific attenuation (γ, dB/km) during the NE monsoon for 40–50 mm/h against ITU-R P.838-3 at 38 GHz under (a) unconstrained winds and (b) constrained winds (9–11 m/s)

The IM season exhibits transitional behavior. The CCDFs in Figures 5 and 6 remain close to ITU-R at 18 GHz, but at 38 GHz, a clearer separation between sectors emerges, especially under constrained winds. This indicates that wind-direction sensitivity can reappear during the

IM, consistent with mixed meteorological conditions that can shift DSD characteristics between events. The constrained-wind statistics in Table 5 capture this directional dependence: the 0°–90° sector has an RMSE of 1.212 dB/km and a bias of +0.936 dB/km, indicating underestimation by ITU-R, whereas the 90°–180° sector shows overestimation (bias = −0.257 dB/km). The presence of both positive and negative bias across directions confirms that the ITU-R error direction is not fixed during the IM. This aligns with prior findings that local rainfall regimes strongly influence DSD behavior and specific-attenuation exceedance statistics [23], and that model errors become more pronounced at mm-wave frequencies when evaluating very-low-time percentages [3, 18].

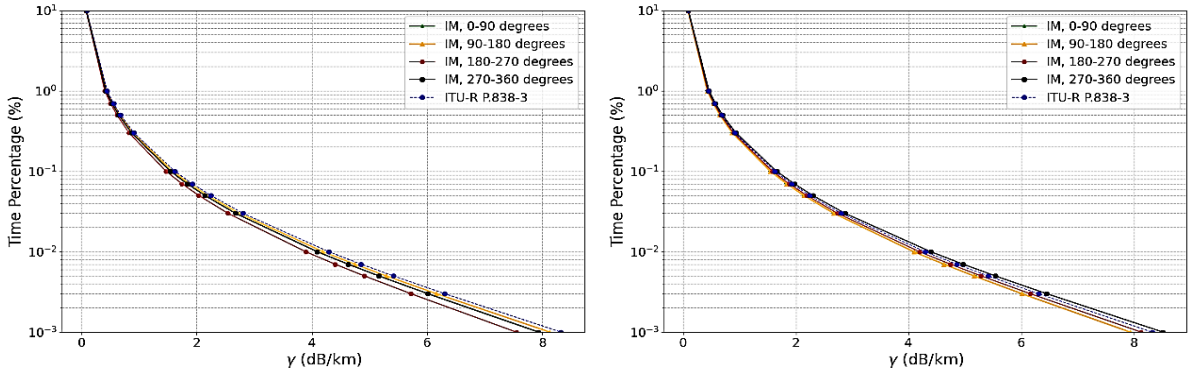

(a) (b)

Figure 5. CCDF of specific attenuation (γ, dB/km) during the IM monsoon for 40–50 mm/h against ITU-R P.838-3 at 18 GHz under (a) unconstrained winds and (b) constrained winds (9–11 m/s)

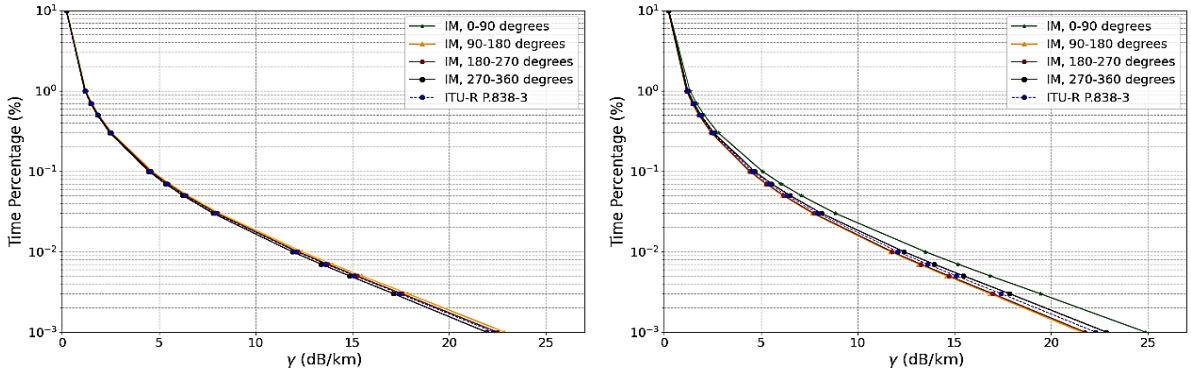

(a) (b)

Figure 6. CCDF of specific attenuation (γ, dB/km) during the IM monsoon for 40–50 mm/h against ITU-R P.838-3 at 38 GHz under (a) unconstrained winds and (b) constrained winds (9–11 m/s)

From a system-design perspective, the practical significance of these findings is tied to the exceedance levels used in link planning. The 0.01% exceedance level (approximately 52.6 min/year under one-minute sampling) is commonly used as a reference for fade-margin planning, while 0.001% (about 5.26 min/year) becomes relevant for more stringent availability targets. The CCDF results show that differences are generally small at 18 GHz, supporting ITU-R as a practical reference at this band. At 38 GHz, however, the largest departures occur under SW and IM in specific wind-direction sectors, precisely where accurate estimation is most critical for reliable operation.

Table 4. RMSE and bias between the DSD-derived specific attenuation and ITU-R P.838-3 at 18 and 38 GHz for 40–50 mm/h under unconstrained winds.

Monsoon	Wind directions [°]	Specific attenuation at 18 GHz [dB/km]		Specific attenuation at 38 GHz [dB/km]	
		RMSE	Bias	RMSE	Bias
SW	**0°–90°**	0.183	-0.136	0.000	0.000
	90°-180°	0.000	0.000	0.107	+0.086
	180°-270°	0.269	+0.207	0.518	−0.393
	270°-360°	0.191	+0.150	1.550	+1.193
NE	**0°–90°**	0.000	0.000	0.601	−0.450
	90°-180°	0.365	-0.279	0.179	−0.121
	180°-270°	0.096	-0.064	0.336	−0.257
	270°-360°	0.183	-0.136	0.107	+0.086
IM	**0°–90°**	0.183	-0.136	0.107	+0.086
	90°-180°	0.096	-0.064	0.254	+0.200
	180°-270°	0.365	-0.279	0.107	+0.086
	270°-360°	0.183	-0.136	0.179	−0.121

A practical example from Malaysia illustrates this relevance, where a 38 GHz system is designed to operate with a specific attenuation of 18.4 dB/km during monsoon conditions [7]. Consistent with the broader literature, prediction errors tend to worsen around 0.01% and 0.001% exceedance levels [1], [17], and underprediction at 30–300 GHz has been reported, particularly below 0.01% [3]. Therefore, the key implication is that fade-margin allocation and link-orientation decisions at 38 GHz in tropical climates should not rely solely on ITU-R; seasonal phase and wind-direction variability can meaningfully affect both the magnitude and the sign of the prediction error.

Table 5. RMSE and bias between the DSD-derived specific attenuation and ITU-R P.838-3 at 18 and 38 GHz for 40–50 mm/h under constrained winds (9–11 m/s)

Monsoon	Wind directions [°]	Specific attenuation at 18 GHz [dB/km]		Specific attenuation at 38 GHz [dB/km]	
		RMSE	Bias	RMSE	Bias
SW	**0°–90°**	0.183	-0.136	0.000	0.000
	90°-180°	0.541	+0.407	1.120	−0.850
	180°-270°	0.269	+0.207	0.107	+0.086
	270°-360°	0.183	-0.136	1.383	−1.050
NE	**0°–90°**	0.000	0.000	0.076	−0.043
	90°-180°	0.183	-0.136	0.433	+0.336
	180°-270°	0.096	-0.064	0.707	+0.550
	270°-360°	0.000	0.000	0.421	−0.314
IM	**0°–90°**	0.183	-0.136	1.212	+0.936
	90°-180°	0.183	-0.136	0.336	−0.257
	180°-270°	0.096	-0.064	0.259	−0.186
	270°-360°	0.107	+0.086	0.254	+0.200

The results indicate that ITU-R P.838-3 performance in a tropical setting is condition-dependent: it is generally adequate at 18 GHz and more reliable during the NE monsoon, but

shows larger, direction-dependent deviations at 38 GHz, especially during the SW and IM periods. For practical 5G/6G mm-wave deployment, this supports using local DSD-derived statistics to (i) identify worst-case wind-direction sectors, (ii) adjust fade margins for the most sensitive seasonal conditions, and (iii) guide link orientation and robustness measures, including alignment tolerance and mounting stability, to reduce outage risk under severe low-exceedance conditions. Importantly, the deviation metrics in Tables 4 and 5 show that the mismatch at 38 GHz can reach RMSE values on the order of 1–1.6 dB/km in the most affected sectors, with the bias sign changing across wind directions, meaning ITU-R may either under- or overestimate depending on the sector. Such sector-dependent behavior cannot be captured by frequency alone and suggests that a rainfall-rate-only framework is insufficient when seasonal variability, wind direction, and wind-driven DSD changes are present. For current 5G links, these deviations may be manageable through conservative margin allocation and practical mitigation, such as tighter alignment tolerance and adaptive fade management. However, as availability targets become more stringent, low-exceedance behavior becomes increasingly critical [27], and adopting monsoon-aware, direction-dependent, and adaptive parameterization will be pivotal to sustaining link performance during fluctuating weather conditions.

4. CONCLUSIONS

This study indicates that the current ITU-R P.838-3 standard does not fully account for the propagation characteristics of tropical rainfall at mm-wave frequencies, which are critical for 5G and future 6G networks. Findings presented in this paper indicate that the greatest discrepancy occurs at 38 GHz during the SW monsoon season, as unconstrained winds lead to excessive specific attenuation relative to the ITU-R predicted values. The 270°–360° sector records the highest deviation under unconstrained winds, with RMSE = 1.550 dB/km and bias = +1.193 dB/km, indicating that ITU-R underestimates the specific attenuation. Under constrained winds (9–11 m/s), the deviation remains high (RMSE = 1.383 dB/km), and the bias becomes sector-dependent. Conversely, during constrained winds, the predicted values are overestimated. During the IM season, there are moderate discrepancies, but they remain sensitive to direction; whereas during the NE monsoon season, the ITU-R values are largely consistent. At 18 GHz, across all seasons and wind conditions, the deviations remain small, with RMSE generally below about 0.6 dB/km and bias values close to zero in all seasons and wind conditions, demonstrating that at this mm-wave band, the ITU-R models could be applied without hassle.

These findings show the effects of factors other than rain rates on specific attenuation, such as seasonal variability, wind direction, and variations in DSD, which introduce complex spatial and temporal dependencies beyond what frequency-only models can account for. The presented results could provide the necessary adaptive requirements for the development of a monsoon-aware, direction-specific fade-margin framework for rainfall prediction models, to warrant high capacity and fulfill stringent availability requirements for 5G and 6G mm-wave links.

ACKNOWLEDGEMENT

This work was conducted as part of the author's doctoral research at the Faculty of Electrical Engineering, Universiti Teknologi Malaysia (UTM), with collaboration from Universiti Tun Hussein Onn Malaysia (UTHM). The author also acknowledges the Ministry of Higher Education (MOHE) and the Department of Polytechnic and Community College Education (DPCCE) for their continuous support. This work received no external research funding.

REFERENCES

[1] S. Shrestha and D.-Y. Choi, "Rain attenuation over terrestrial microwave links in South Korea," Iet Microwaves Antennas & Propagation, vol. 11, no. 7, pp. 1031–1039, Jun. 2017, doi: 10.1049/IET-MAP.2016.0553.

[2] J. Tan and M. Thurai, "Rain-induced cross polarisation on line-of-sight systems at 38 GHz," vol. 144, no. 1, pp. 20–26, Feb. 1997, doi: 10.1049/IP-MAP:19970962.

[3] I. Mata-Alonso, J. M. Riera, L. Luini, H. Y. Lam, and D. Pimienta-del-Valle, "Rain Attenuation at Millimeter Waves in Different Climatic Zones Estimated from Drop Size Distributions," pp. 1–5, Mar. 2024, doi: 10.23919/eucap60739.2024.10501081.

[4] M. Rashid, J. Din and O. A. Aziz, " Spatial variations of rain intensity over a short length propagation for 5G links based on a rain gauge network", doi: 0.12928/TELKOMNIKA.v19i2.16809.

[5] H. Y. Lam, J. Din, and S. L. Jong, "Statistical and Physical Descriptions of Raindrop Size Distributions in Equatorial Malaysia from Disdrometer Observations," Advances in Meteorology, vol. 2015, pp. 1–14, 2015, doi: https://doi.org/10.1155/2015/25373.

[6] H. Y. Lam, L. Luini, J. Din, M. J. Alhilali, S. L. Long, and F. Cuervo, "Impact of rain attenuation on 5G millimeter-wave systems in equatorial Malaysia investigated through disdrometer data," in Proc. EuCAP 2017, pp. 1793-1707, 2017, doi: 10.23919/EuCAP.2017.7928616.

[7] I. A. Shayea, S. A. Alkhawaldeh, M. A. Nisirat, T. A. Rahman, and M. Ergen, "Channel fading attenuation based on rainfall rate for future 5G wireless communication system over 38-GHz," International Journal of Electrical and Computer Engineering (IJECE), vol. 12, no. 5, p. 5104, Oct. 2022, doi: https://doi.org/10.11591/ijece.v12i5.pp5104-5113.

[8] H. Y. Lam, L. Luini, J. Din, C. Capsoni, and A. D. Panagopoulos, "Investigation of Rain Attenuation in Equatorial Kuala Lumpur," IEEE Antennas and Wireless Propagation Letters, vol. 11, pp. 1002–1005, 2012, doi: https://doi.org/10.1109/lawp.2012.221437.

[9] Asma Ali Budalal et al., "Effective Rain Rate Model for Analysing Overestimated Rain Fade in Short Millimetre-Wave Terrestrial Links Due to Distance Factor," Results in Engineering, pp. 104112–104112, Jan. 2025, doi: https://doi.org/10.1016/j.rineng.2025.104112.

[10] F. A. Semire, R. Mohd-Mokhtar, and I. A. Akanbi, "Validation of New ITU-R Rain Attenuation Prediction Model over Malaysia Equatorial Region," MAPAN, vol. 34, no. 1, pp. 71–77, Nov. 2018, doi: https://doi.org/10.1007/s12647-018-0295-z.

[11] H Ju, Y Zou and G.M. Rebeiz, " A 6–19 GHz Reconfigurable I/Q Receiver with 21 dB Gain, 3 dB NF, and 30 dB IRR for 6G FR3 in 22-nm FD-SOI," 2025 IEEE BiCMOS and Compound Semiconductor Integrated Circuits and Technology Symposium (BCICTS), San Diego, USA, 2025, pp. 1-4, doi: https://doi.org/10.1155/2019/1712791.

[12] B. B. Jimoh, A. Y. Abdulrahman, A. J. Falade, O. Oniyide, S. O. Zakariyya, and T. A. Rahman, "Evaluation of the frequency scaling prediction techniques using experimental data," Telecommunications and Radio Engineering, vol. 76, no. 5, pp. 433–442, Jan. 2017, doi: https://doi.org/10.1615/telecomradeng.v76.i5.40.

[13] M. Woldamanuel and F. D. Diba, "Enhanced adaptive code modulation for rainfall fade mitigation in Ethiopia," EURASIP Journal on Wireless Communications and Networking, vol. 2022, no. 1, Jan. 2022, doi: https://doi.org/10.1186/s13638-021-02085-0.

[14] P. Valtr, M. Fencl, V. Bareš and P. Pechač, "Comparison of measured and theoretically predicted rain attenuation at 32 GHz and 38 GHz," 12th European Conference on Antennas and Propagation (EuCAP 2018), London, UK, 2018, pp. 1-3, doi: 10.1049/cp.2018.0377.

[15] M. R. Islam, J. Chebil, O. O. Khalifa, S. Khan, H. Dao and A. -H. Zyoud, "Effect of frequency on fade slope based on rain attenuation data measured in malaysia," International Conference on Computer and Communication Engineering (ICCCE'10), Kuala Lumpur, Malaysia, 2010, pp. 1-4, doi: 10.1109/ICCCE.2010.5556834.

[16] F. Capelletti and L. Luini, "An Effective Approach to Instantaneous Rain Attenuation Frequency Scaling Using Single or Multiple Satellite-Based Measurements," in IEEE Transactions on Antennas and Propagation, vol. 73, no. 7, pp. 4853-4862, July 2025, doi: 10.1109/TAP.2025.3552227.

[17] M. Ghanim, M. Alhilali, J. Din, and H. Y. Lam, "Rain attenuation statistics over 5G millimetre wave links in Malaysia," Indonesian Journal of Electrical Engineering and Computer Science, vol. 14, no. 2, p. 1012, May 2019, doi: https://doi.org/10.11591/ijeecs.v14.i2.pp1012-1017.

[18] A. Kumar Verma, R. Nandan and A. Verma, "Regional variability of Specific rain attenuation in mm wave region for Indian Sub-tropical climate," 2018 IEEE Indian Conference on Antennas and Propogation (InCAP), Hyderabad, India, 2018, pp. 1-4, doi: 10.1109/INCAP.2018.8770886.

[19] A. M. Al-Saegh, A. Sali, J.S. Mandeep, and A. Ismail, "Extracted atmospheric impairments on earth-sky signal quality in tropical regions at Ku-band," Journal of Atmospheric and Solar-Terrestrial Physics, vol. 104, pp. 96–105, Sep. 2013, doi: https://doi.org/10.1016/j.jastp.2013.08.018.

[20] A. Aresu, P. Martellucci and P. Migliorini, "Depolarizing properties of rain, measured on a 30 GHz short path terrestrial link," International Symposium on Antennas and Propagation Society, Merging Technologies for the 90's, Dallas, TX, USA, 1990, pp. 1824-1827 vol.4, doi: 10.1109/APS.1990.115486.

[21] A. M. Al-Saegh, A. Sali, M. Singh, A. Ismail, and A. H. J. Aljumaily, "Earth-sky link quality performance for fixed and mobile scenarios in tropical regions," Progress In Electromagnetics Research C, vol. 39, pp. 61–75, 2013, doi: https://doi.org/10.2528/pierc13022703.

[22] N. N. Md Yusof, J. Din, and H. Y. Lam, "Enhancing millimeter-wave communication: a tropical perspective on raindrop size distribution and signal attenuation," International Journal of Power Electronics and Drive Systems, vol. 15, no. 1, p. 467, Nov. 2024, doi: 10.11591/ijece.v15i1.pp467-479

[23] Y. Li, Y. Zheng, G. Chen, L. Li and F. Xu, "Difference analysis of raindrop size distribution characteristics in Meiyu and typhoon types of short-term heavy rainfall in summer in Jiangsu Province," Transactions of Atmospheric Sciences, vol. 47, no. 5, pp. 798-808, 2024, doi: 10.13878/j.cnki.dqkxxb.20240422002

[24] M. Rashid, J. Din, H. Y. Lam and O. A. Aziz, "Preliminary Investigation of Small Scale Spatial Variability of Rain Intensity Using a Rain Gauge Network for Mm-Wave Propagation Application," *2021 IEEE Asia-Pacific Conference on Applied Electromagnetics (APACE)*, Penang, Malaysia, 2021, pp. 1-5, doi: 10.1109/APACE53143.2021.9760672

[25] Z. Saberi, A. Fudholi and K. Sopian, "Fitting of weibull distribution method to analysis wind energy potential at Kuala Terengganu, Malaysia," Journal of Advanced Research in Fluid Mechanics and Thermal Sciences, vol. 66, no. 1, pp. 1-11, Feb 2020,

[26] Y. A. Ahmad, A. F. Ismail, A. Hamid, and M. F. Jamlos, "Area-Based Rainfall Rate Model for Specific Attenuation in the Equatorial Region," IIUM Engineering Journal, vol. 25, no. 2, pp. 287–298, Jul. 2024, doi: https://doi.org/10.31436/iiumej.v25i2.3279

[27] A. Shukur, Y. A. Ahmad, Muhammad, and Khairayu Badron, "Latency Performance Evaluation of LEO Starlink and SES-12 GEO HTS Network Under Tropical Rainfall Conditions," IIUM Engineering Journal, vol. 26, no. 2, pp. 204–219, May 2025, doi: https://doi.org/10.31436/iiumej.v26i2.3653.